Supplementary Information

1. Data density

Figure S1 shows the resolution and number of records contributing to the SST and $\delta^{18}O_{sw}$ stacks through time. Most records cover the last glacial cycle, but the number declines considerably further back in time. Similarly, the resolution of the records degrades with age from an average of 1.5 to 5 kyr over 0-800 ka.

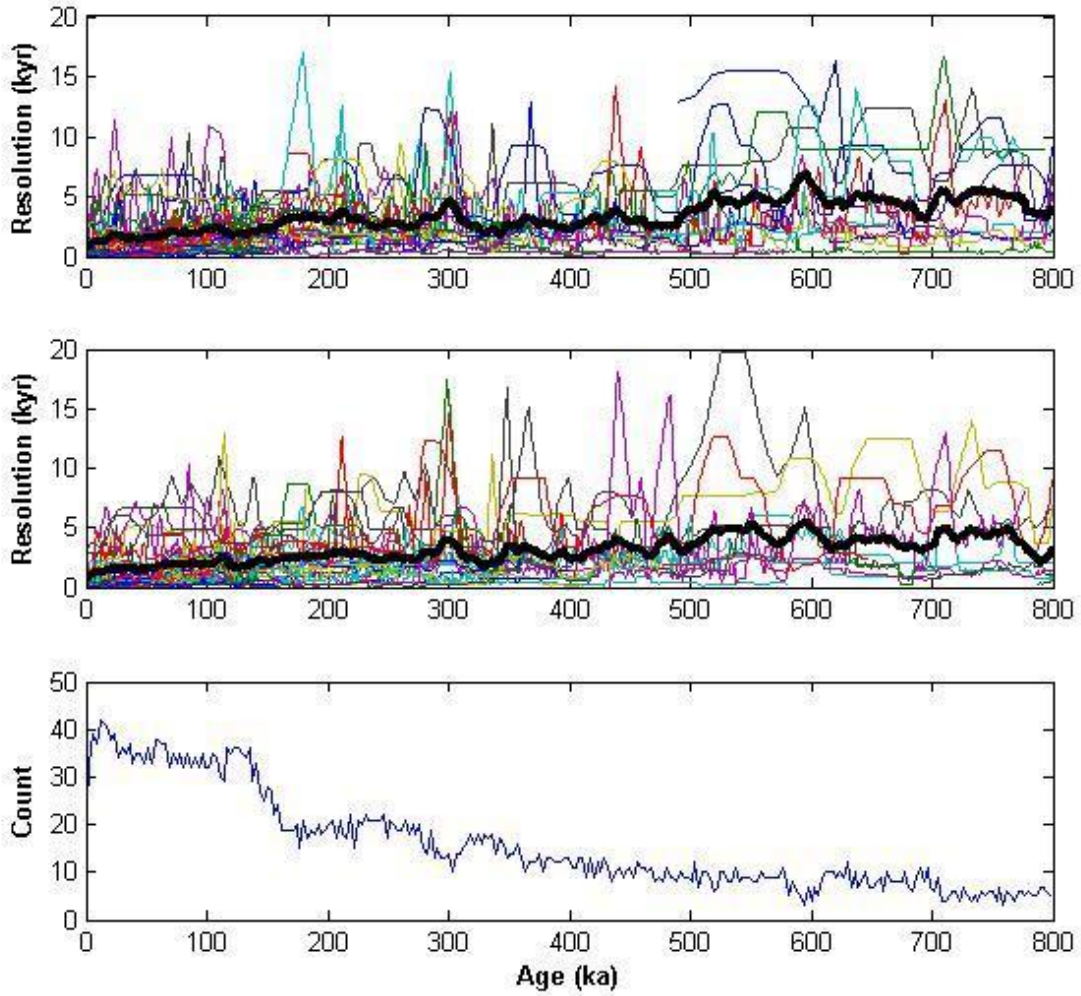

731

732 **Fig. S1.** Resolutions of individual (**a**) SST and (**b**) $\delta^{18}O_p$ records over the past 800 kyr are shown as

733 colored lines, and black lines give average resolution. (**c**) Number of $\delta^{18}O_{sw}$ records contributing to the

734 stack through time.

735

736

737

738

739 **2. 800-kyr stacks**

We show a closer comparison of the stacks generated in this study here, as well as the partitioning of the $\delta^{18}O_c$ record into its early temperature and late $\delta^{18}O_{sw}$ components. The $\delta^{18}O_b$ stack is very similar to the LR04 benthic stack, as expected since these data were correlated to LR04 (r^2=0.96) (Figure S2a). The glacial-interglacial amplitude is slightly smaller in the $\delta^{18}O_b$ stack than LR04 though (slope of regression=0.88), perhaps because LR04 contains a greater proportion of Atlantic records. The $\delta^{18}O_p$ stack is also quite similar to the benthic stacks (slope of regression with LR04=0.84, r^2=0.86) (Figure S2a), reflecting a close relationship between temperature and salinity changes in the surface and deep ocean over glacial cycles. A notable exception, however, is that the MIS 7, 9, and 11 interglacials are smaller in $\delta^{18}O_p$ than $\delta^{18}O_b$. This discrepancy is unlikely to reflect smoothing of interglacial peaks in $\delta^{18}O_p$ due to chronological errors because the records were aligned using $\delta^{18}O$ and instead must be due to less warming or freshening at the sea surface during these interglacials.

A comparison of the $\delta^{18}O_p$ stack with the SST stack, scaled to $\delta^{18}O_c$-equivalent using 0.25‰ per °C, shows that temperature accounts for most of the variability in marine $\delta^{18}O_c$ early in glacial cycles (Figure S2b), while $\delta^{18}O_{sw}$ explains most of the variability in marine $\delta^{18}O_c$ during the latter part of glacial cycles (Figure S2c). Subtracting the $\delta^{18}O_{sw}$ stack from the LR04 stack, on the assumption that $\delta^{18}O_{sw}$ varied in concert between the surface and deep ocean, yields a bottom water temperature signal that likewise accounts for most of the variability in marine $\delta^{18}O_b$ during the first half of glacial cycles (Figure S2d).

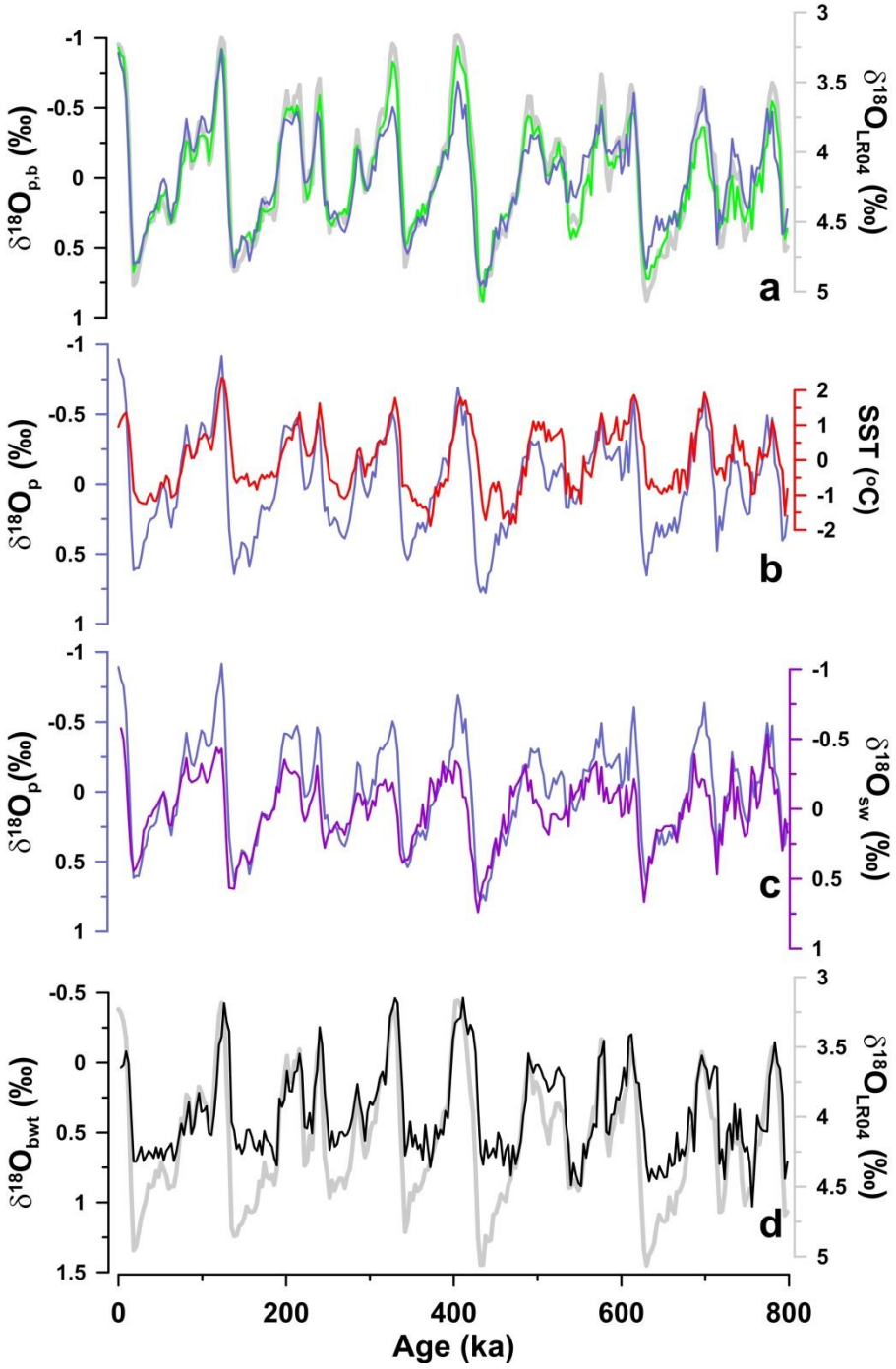

759

760

761 **Fig. S2.** (**a**) The $\delta^{18}O_p$ (blue) and $\delta^{18}O_b$ (green) stacks from the dataset used in this study and the LR04

762 stack (gray). (**b**) The $\delta^{18}O_p$ (blue) and SST (red) stacks. Their axes are scaled proportionally, such that 1°C

763 = 0.25‰. (**c**) The $\delta^{18}O_p$ stack (blue) and planktic $\delta^{18}O_{sw}$ stack (purple). (**d**) Bottom water temperature

($\delta^{18}O_{bwt}$) (black) contribution to the LR04 stack (gray), calculated as the difference between the planktic $\delta^{18}O_{sw}$ and LR04 stacks. All time series, except LR04 and $\delta^{18}O_{bwt}$, have been shifted to have a mean of zero; $\delta^{18}O_{bwt}$ has been shifted to have a Holocene value of 0‰. Approximately half of the variability in $\delta^{18}O_{p}$ is unaccounted for by SST, particularly during the latter part of glacial cycles, and must be attributable to $\delta^{18}O_{sw}$.

3. Ice volume model

3.1. Parameter sensitivity tests

We tested the sensitivity of the Imbrie and Imbrie (1980) model results using combined insolation-SST forcing, shown in Figure 8d in the manuscript, to variations in the ice-sheet time constant (Tm) and ice growth-decay asymmetry parameter (b). The model output is dominated by a 100-kyr cycle and only small shifts in phase occur across a broad range of parameter choices, which largely serve to control the amount of precession variability (Figure S3).

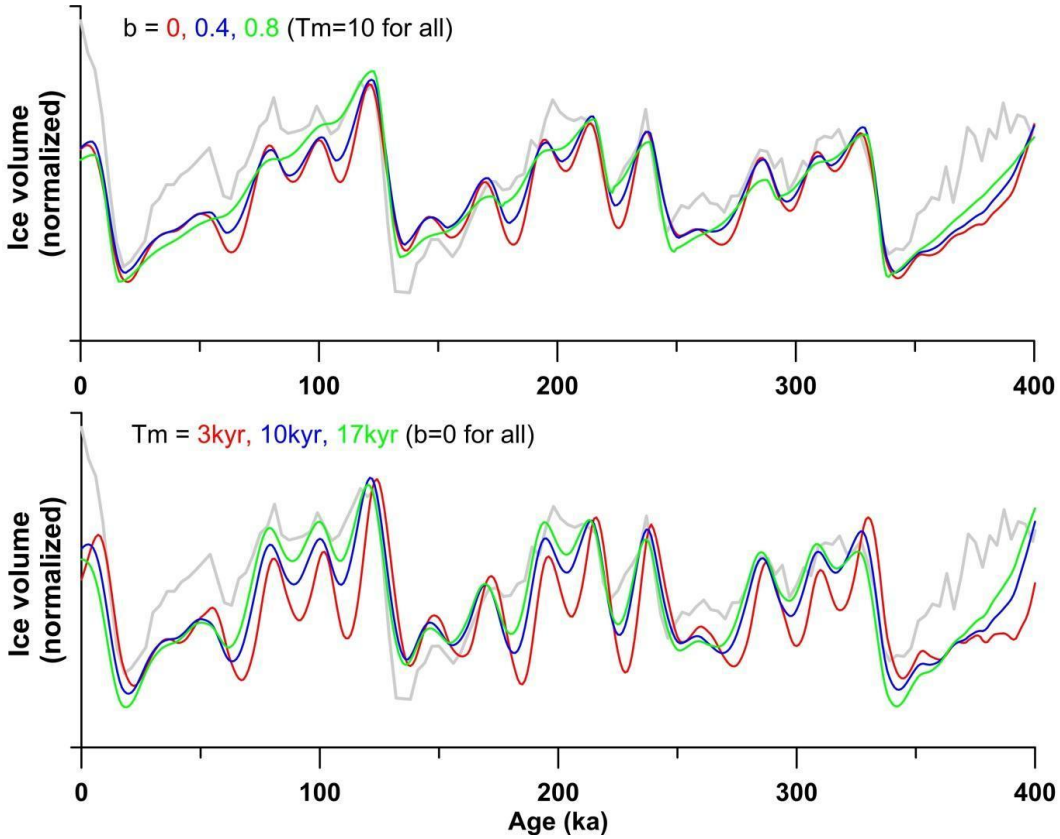

Fig. S3. Results of running the Imbrie and Imbrie (1980) ice volume model with various ice growth-decay asymmetry parameters (b) and ice-sheet time constants (Tm). The model was forced by the average of normalized global SST and 65°N June 21 insolation variations. The global planktic $\delta^{18}O_{sw}$ stack is shown by the gray line.

3.2. The last 3 Myr

We also extended the Imbrie and Imbrie (1980) modeling results to the last 3 Myr. More specifically, the high latitude surface air temperature reconstruction of Bintanja and van de Wal (2008) and 65°N June 21 insolation curve were normalized and averaged, and used as the input function to the model. The model output exhibits the major features of the marine $\delta^{18}O$ record, including dominantly 41-kyr cycles in the early Pleistocene and larger, 100-kyr cycles in the late Pleistocene (Figure S4), suggesting that consideration of temperature in addition to insolation may help to explain the pattern of

790 Pleistocene glaciation (Raymo, 1997). Note that Bintanja and van de Wal's (2008) temperature
791 reconstruction is derived from the marine $\delta^{18}O$ record through inverse ice-sheet modeling, and thus
792 adds an element of circularity to our argument. Nonetheless, a Plio-Pleistocene tropical SST stack
793 supports the general temperature progression seen Bintanja and van de Wal's (2008) reconstruction,
794 with a long-term cooling trend and a shift from 41 to 100-kyr cycles (Herbert et al., 2010).
795

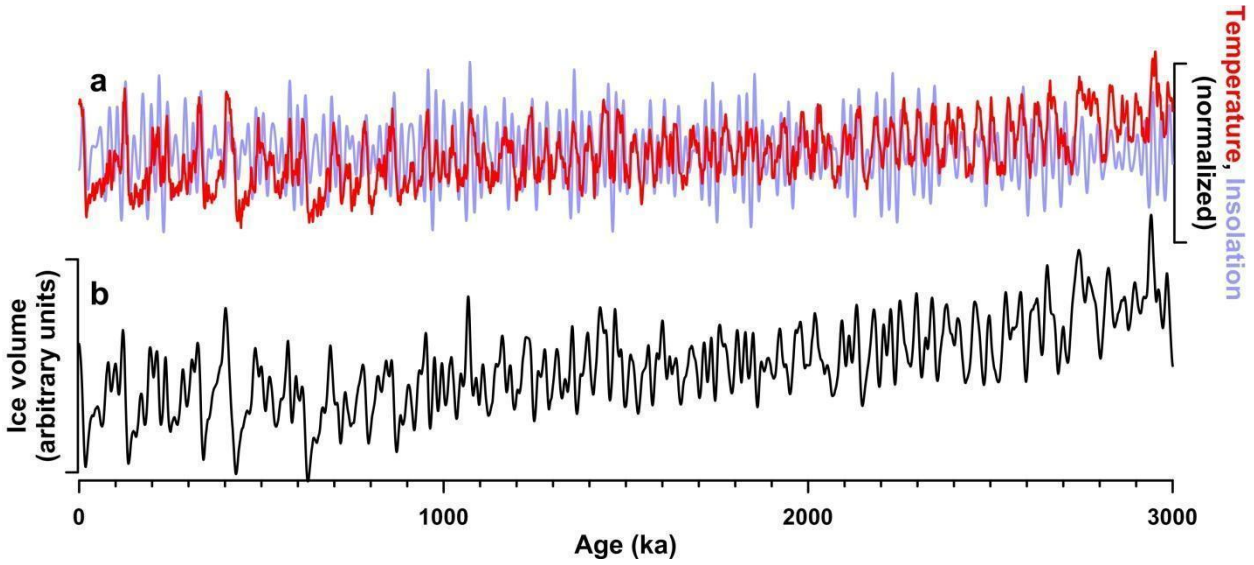

796

797 **Fig. S4.** (**a**) Inverse-modeled high latitude surface air temperature (red) (Bintanja and van de Wal, 2008)
798 and 65°N insolation on June 21 (blue) (Laskar et al., 2004). Both time series have been normalized to
799 mean zero, unit variance. (**b**) Ice volume simulated with the Imbrie and Imbrie (1980) model forced by
800 the average of the temperature and insolation time series in (a), and assuming an ice sheet time
801 constant of 17 kyr and ice growth-decay asymmetry parameter of 0.
802
803
804 **Supplementary References**
805 Bintanja, R., van de Wal, R.S.W., 2008. North American ice-sheet dynamics and the onset of 100,000-
806 year glacial cycles. Nature 454, 869-872.

807 Herbert, T.D., Peterson, L.C., Lawrence, K.T., Liu, Z., 2010. Tropical Ocean Temperatures Over the Past
808 3.5 Million Years. Science 328, 1530-1534.
809 Imbrie, J., Imbrie, J.Z., 1980. Modeling the climatic response to orbital variations. s 207, 943-953.
810 Laskar, J., Robutel, P., Joutel, F., Gastineau, M., Correia, A.C.M., Levrard, B., 2004. A long term numerical
811 solution for the insolation quantities of the Earth. Astronomy and Astrophysics 428, 261-285.
812 Raymo, M.E., 1997. The timing of major climate terminations. Paleoceanography 12, 577-585.
813
814
815